

**IMECE2005-81824**

**KINEMATICS AND DYNAMICS OF NANOSTRUCTURED ORIGAMI™**

P. Stellman<sup>(1)</sup>  
stellman@mit.edu

S. Takahashi<sup>(1)</sup>  
takahash@mit.edu

E.D. Demaine<sup>(2)</sup>  
edemaine@mit.edu

W. Arora<sup>(2)</sup>  
will@nano.mit.edu

G. Barbastathis<sup>(1)</sup>  
gbarb@mit.edu

<sup>(1)</sup> Department of Mechanical Engineering  
Massachusetts Institute of Technology  
Cambridge, MA 02139

<sup>(2)</sup> Department of Electrical Engineering and  
Computer Science  
Massachusetts Institute of Technology  
Cambridge, MA 02139

**ABSTRACT**

Two-dimensional (2D) nanofabrication processes such as lithography are the primary tools for building functional nanostructures. The third spatial dimension enables completely new devices to be realized, such as photonic crystals with arbitrary defect structures and materials with negative index of refraction [1]. Presently, available methods for three-dimensional (3D) nanopatterning tend to be either cost inefficient or limited to periodic structures. The Nanostructured Origami method fabricates 3D devices by first patterning nanostructures (electronic, optical, mechanical, etc) onto a 2D substrate and subsequently folding segments along predefined creases until the final design is obtained [2]. This approach allows almost arbitrary 3D nanostructured systems to be fabricated using exclusively 2D nanopatterning tools.

In this paper, we present two approaches to the kinematic and dynamic modeling of folding origami structures. The first approach deals with the kinematics of unfolding single-vertex origami. This work is based on research conducted in the origami mathematics community, which is making rapid progress in understanding the geometry of origami and folding in general [3]. First, a unit positive “charge” is assigned to the creases of the structure in its folded state. Thus, each configuration of the structure as it unfolds can be assigned a value of electrostatic (Coulomb) energy. Because of repulsion between the positive charges, the structure will unfold if allowed to decrease its energy. If the energy minimization can be carried out all the way to the completely unfolded state, we are simultaneously guaranteed of the absence of collisions for the determined path.

The second method deals with dynamic modeling of folding multi-segment (accordion style) origamis. The actuation method for folding the segments uses a thin, stressed metal layer that is deposited as a hinge on a relatively stress free structural layer. Through the use of robotics routines, the hinges are modeled as revolute joints, and the system dynamics are calculated.

Keywords: nanomanufacturing, self-assembly, origami, dynamics, control

**INTRODUCTION**

Fabrication of 3D nanostructures is a challenging endeavor since most of the tools used in industry and research employ 2D processes. Conventional 2D patterning methods such as electron beam lithography can be used to write feature sizes on the order of 20 nm [4], but the utility of these structures is limited in part by their planar geometry. Manufacturing nanostructures in three spatial dimensions introduces added functionality since the volume enclosed by the device can be used as an additional design parameter.

Nature is currently the most efficient 3D nanomanufacturer. Proteins, for example, are 1D structures that are folded via self-assembly into 3D machines. The effectiveness of protein mechanics originates from its unique three-dimensional geometry. The Nanostructured Origami method (Fig. 1) exploits 3D in nanomanufacturing by patterning devices and hinges in 2D and folding them into a desired 3D structure. This manufacturing technique is inspired by the Japanese art of origami, in which creases are first patterned in paper and then folded into the final shape. Just as proteins fold to make useful

devices, man-made nanostructures would benefit from folding as well. Hybrid devices with electronic, optical, electrical, and fluidic components could potentially be integrated into a self-assembled, compact design, and optical devices such as photonic crystals and optical interconnects could be fabricated efficiently.



**Fig. 1 Nanostructured Origami Concept**

In order to realize complex structures, a solid theoretical understanding of origami design and actuation is necessary. This paper describes an initial theoretical investigation into the design and control of Nanostructured Origami from the perspective of both origami mathematics and system dynamics. This dual approach tackles difficult geometric questions about origami in general, and it tests the scalability of systems theory to the fabrication of nanostructured devices. The first section of this paper identifies design questions associated with the unfolding of single vertex origami and proposes a solution based on previous results from the burgeoning field of origami mathematics. The second theoretical topic presented in this report models the dynamics of accordion-style origami using techniques developed for the robotics community.

## NOMENCLATURE

$A$  - area of origami segment  
 $B$  - drag matrix  
 $C$  - Coriolis matrix  
 $C_D$  - drag coefficient  
 $E_i$  - Young's modulus of film layer  $i$   
 $J$  - Jacobian matrix  
 $K$  - torsional stiffness matrix  
 $L$  - length of origami flap  
 $M$  - equivalent mass matrix  
 $M$  - mass matrix  
 $U$  - energy function  
 $d$  - geodesic distance along the unit sphere  
 $g$  - rigid body transformation matrix  
 $l$  - length of hinge  
 $q$  - point on twist axis

$t_i$  - thickness of film layer  $i$   
 $w$  - width of hinge  
 $\beta$  - etch rate  
 $\gamma$  - arc length  
 $\varepsilon$  - residual strain  
 $\zeta$  - twist  
 $\theta$  - generalized coordinate for joint; turn angle  
 $\lambda$  - Lagrange multipliers  
 $\rho$  - radius of curvature  
 $\tau$  - applied torque  
 $v$  - density  
 $\varphi$  - zenith coordinate for sphere  
 $\psi$  - azimuthal coordinate for sphere  
 $\omega$  - twist axis

## UNFOLDING OF SINGLE-VERTEX ORIGAMI

For the purposes of Nanostructured Origami, the folded configuration of a structure is typically known since the device's geometry is dictated by a design's functional requirements. One question that arises addresses the manufacturability of the final shape. Because the patterning step is constrained by 2D writing methods, the origami must be foldable from a plane. Further manufacturing requirements restrict the folding motion to be continuous throughout its configuration space while disallowing self-intersection of the origami flaps. Thus, the objective is to determine if it is possible to smoothly fold an origami from 2D to 3D without collisions. An energy-based algorithm that has answered this kinematic design question for the case of all single-vertex origami (origami with creases that intersect at a single point) will be presented. Instead of modeling the *folding*, however, the algorithm tests whether a desired 3D origami is flat *unfoldable* by taking advantage of already knowing its final state. The unfolding is therefore a unique path that is consistent with the direction of rotation about the creases.

### Energy Methods for Unfolding

Much of the work on the unfolding of single vertex origami is based on methods for unfolding linkages. Connelly, Demaine, and Rote proved that there are no locked chains in 2D [5]. The physical meaning of this proof is that no two configurations of a chain in two dimensions can be prevented from reaching one another via continuous motions. The obvious question that arises is whether there is an algorithm that can convexify or straighten an arbitrary 2-D linkage. Prior work by Connelly, et al [6], and Streinu [7] have answered this question in the affirmative, but the fastest method found to date algorithmically

was described in 2004 by Cantarella, Demaine, Iben, and O'Brien [8]. The proposed algorithm assigns a repulsive energy function to a graph of  $n$  vertices that are parameterized to maintain constant edge lengths. The algorithm then follows the steepest descent of energy until the chain has been convexified or straightened.

The inspiration for using an energy method to model the kinematics of single-vertex origami came from both [8] and research recently reported by Streinu and Whiteley [9]. The proof in [9] shows that every simple, single-vertex origami fold with the fold-vertex interior to the paper, interior to a boundary edge, or situated at a convex vertex can be unfolded with expansive motions. The proof was based on motion of circular arcs along a spherical surface. This result implies that, since expansive motions exist, there should be an algorithm for unfolding along the sphere.

The model implemented in this report uses the mathematical convenience of origami motions along the unit sphere. The idea is to use spherical arcs in the plane of the origami flaps whose nodes lie on the crease lines at unit length from the center vertex of the origami. Since the arc lengths are always kept at unit length from the center, every motion of an arc is exactly along the unit sphere. Fig. 2 illustrates the model in both the flat and folded states for the corner cube, and it shows the spherical coordinate frame used in the calculations.

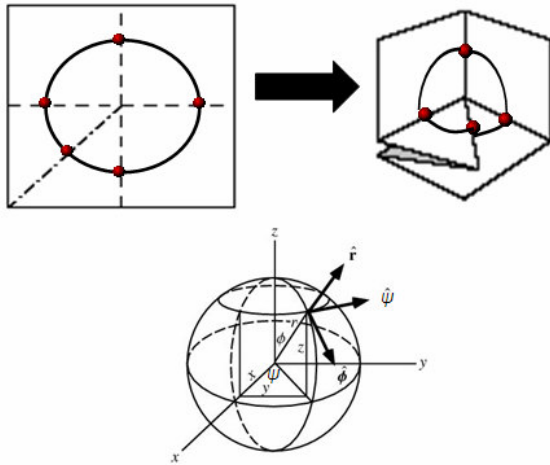


**Fig. 2 Charge model for corner cube and spherical coordinates**

Both the nodes of the bars (shown in red in Fig. 2) and the midpoints of each spherical arc are represented mathematically as unit, positive, electrostatic charges. The electrostatic potential induces a global energy field that tends to repel nodes from the arcs until the energy is minimized by following the steepest descent of energy.

[8] proposed a set of four criteria that an admissible energy function should meet to smoothly unfold a chain. The properties include charge, repulsive, separable, and continuous first and second derivatives. The charge property indicates that the energy function tends to infinity if any two bars cross. Repulsive means that the vertices should repel each other as the energy is minimized, and separable specifies that the components of the energy function should be independent.

The simulations reported in this paper tested both admissible energy functions described above and energy functions that met only the repulsive and continuity requirements. Equations 1 and 2 illustrate the form for both the separable and non-separable cases, respectively. The energy is thus inversely proportional to the geodesic distance,  $d$ , along the unit sphere between each node and the center of every non-adjacent spherical arc, where  $p$  is a positive, real number. It is interesting to note that both types of energy functions led the origami to unfold, but each encountered a few local minima, especially in the case of the corner cube.

$$U = \sum_{\substack{\text{arc } e \\ \text{node } v \notin e}} \frac{1}{d(v, e)^p} \quad (1)$$

$$U = \frac{1}{\sum_{\substack{\text{arc } e \\ \text{node } v \notin e}} d(v, e)^p} \quad (2)$$

The geodesic distance along the sphere was calculated using the cosine rule of spherical trigonometry. Spherical coordinates are depicted in Fig. 2 above, where the unit directions are  $r$ ,  $\psi$ , and  $\phi$ . The arc lengths,  $\gamma$ , are of fixed length as defined in Eq. 3 for an arc beginning at node  $v_i$  and terminating at node  $v_{i+1}$ .

$$\cos(\gamma_i) = \cos(\phi_i)\cos(\phi_{i+1}) + \sin(\phi_i)\sin(\phi_i)\cos(\psi_{i+1} - \psi_i) \quad (3)$$

The energy functions defined in Eq. 1 and 2 were minimized by numerically solving the Kuhn-Tucker equations (Eq. 4-6) using optimization routines in MATLAB. The rigid arc length constraint is represented by the vector  $G$ , and Lagrange multipliers are introduced to ensure that the system of equations remains in equilibrium. In the implementation,  $p=2$  and  $p=4$  produced the smoothest results for the separable and non-separable, respectively.

$$\nabla U(\psi_i, \phi_i) + \sum_{i=1}^m \lambda_i \cdot \nabla G_i(\psi_i, \phi_i) = 0 \quad (4)$$

$$\lambda_i \cdot G(\psi_i, \phi_i) = 0, i = 1..m \quad (5)$$

$$\lambda_i \geq 0 \quad (6)$$

### Simulation Results

For an origami design to be manufacturable in a geometric sense, it must be foldable from 2D while ensuring that the flaps of the origami remain rigid. The constraint definition in the Kuhn-Tucker equations maintains the flap rigidity, and the energy function drives the charges to unfold to a plane in the shape of a circle. If the final state of the charges is not in the plane, then the initial folded state is either knotted or not flat unfoldable. The repulsive property of the energy function also prevents the flaps from intersecting, meaning that there exists at least one collision-free folding path. Although the topology of a single-vertex origami is relatively simple, it is possible that similar energy-based methods could aid in the design of multiple vertex origami or in the dynamical analysis of origami.

Simulation results rendered in OpenGL are illustrated in the unfolding trajectories of Fig. 3a and 3b. The corner cube in Fig. 3a is an especially useful single-vertex origami because it could be manufactured with applications as a reflective optical device.

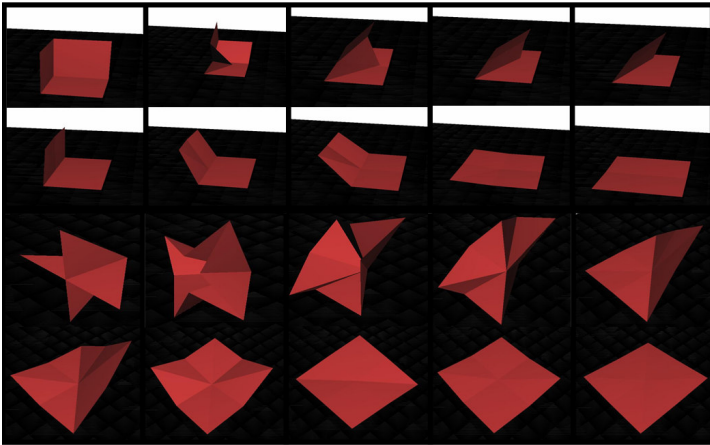


**Fig. 3 a.) Corner cube charge method unfolding; b.) Waterbomb base unfolding**

### DYNAMICS OF ACCORDION ORIGAMI

The previous discussion considered geometrical aspects of origami design. Actuating a nanostructured device, on the other hand, requires a detailed physical model of the geometry and materials used in fabrication. The dynamic equations of motion for the system can then be derived, and a control scheme can be implemented. The results from the equations of motion then represent the physical path traversed, and the resulting generalized forces can be calculated. The actuation method used in the laboratory represents an external input to the system, which must also be modeled according to the fabrication techniques. Once a model of the origami and the input is formulated, design iterations can be performed prior to and during fabrication.

### Stress Actuation Method

One method of folding nanopatterned membranes is to deposit stressed chromium as a hinge on a structural layer of silicon nitride. Upon release from the silicon substrate in a potassium hydroxide (KOH) etch bath, the stressed bilayer bends the device to a radius of curvature described by the relationship in Eq. 7 [10]. The radius of curvature of the bending bilayer is a fundamental property for a set of given material properties, residual strain, and film thicknesses. The remaining hinge property yet to be defined is the initial length,  $l$ , of the hinge, which is found by the simple relationship  $l = \rho\theta$ , where  $\theta$  is the turn angle of the film.

$$\rho = \frac{1}{k} = \frac{E_1'^2 t_1^4 + E_2'^2 t_2^4 + 2E_1' E_2' t_1 t_2 \cdot (2t_1^2 + 3t_1 t_2)}{6E_1' E_2' t_1 t_2 (t_1 + t_2) \cdot (C/E_2')} \quad (7)$$

Results from [11] are shown below in Fig. 4, which demonstrates the ability to fold thin films to an arbitrary angle. The trenches shown in the SEM images are results of the slow KOH etch procedure. The anisotropy of the etch allows the Cr hinge to fold largely about only one revolute axis. This allows for an easy parameterization of more complex devices in terms of twists and the product of exponentials formula [12].

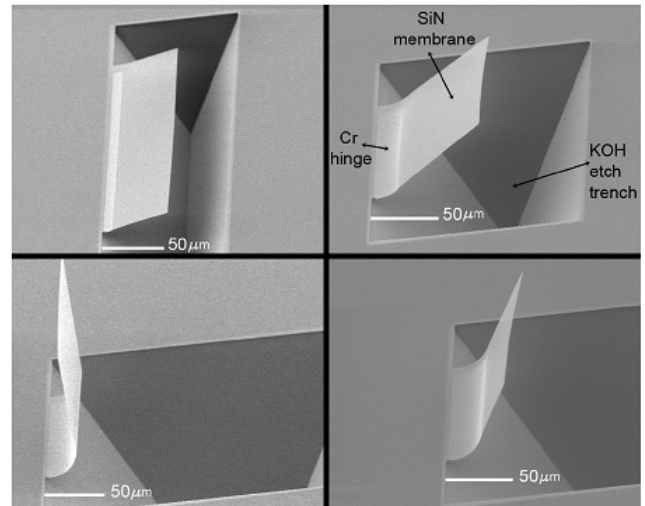


**Fig. 4 200 nm thick silicon nitride membranes with 100 nm thick Cr hinges are folded to arbitrary angles between 0 and 90 deg using stress actuation method**

### Accordion Origami Model and Kinematics

An accordion origami is a simple example of the applicability of the Nanostructured Origami technique. Photonic crystals (Fig. 5a) and other layered devices could be fabricated by patterning in 2D and folding into 3D. A working 6 level electrochemical supercapacitor, shown in Fig. 5b, demonstrates the utility of the accordion origami design [13].

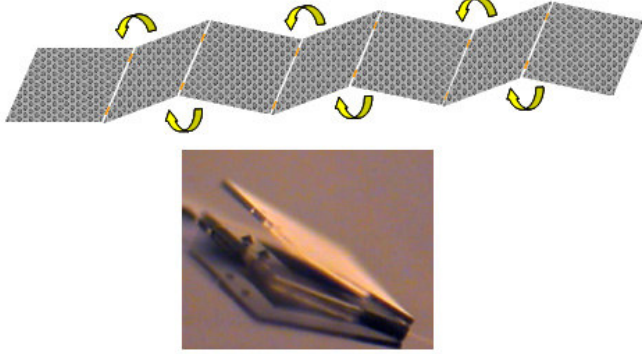


**Fig. 5 a.) Origami fabrication schematic for photonic crystals; b.) Electrochemical supercapacitor as an example of an actual device**

Consider the model of a 3-flap accordion origami in Fig. 6. The inertial coordinate frame is located at  $A$ , and the body frames of each flap are shown in the figure. In order to calculate the origami's dynamics, the center of gravity (CG) of each link must be parameterized with respect to the inertial frame  $A$ .

In order to define a linkage in terms of twists, the axes of rotation and a point on that axis must be defined with respect to  $A$ . The unit vector,  $\omega_i$ , for the rotation axes and the points,  $q_i$ , on those axes are defined below. In this model, the axes of rotation lie in the plane of the origami flaps, but in reality, the radius of curvature introduces a certain clearance between the layers, which should be addressed in the future.

The forward kinematics map (Eq. 8) representing the configuration of a linkage with respect to  $A$  is given by the product of exponentials formula. The rigid body transformation,  $g$ , is a 4x4 homogeneous coordinate transformation in the special Euclidean group,  $SE(3)$ . This expression is used as the parameterization for the generalized coordinates used in the

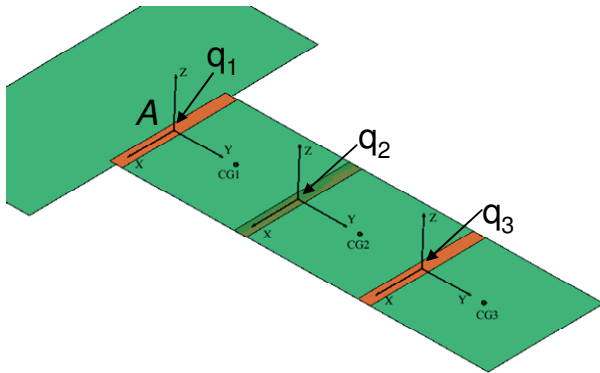


**Fig. 6 Model of accordion origami**

equations of motion. Equation 9 illustrates the initial rigid body configuration of the CGs of each origami segment in  $A$ 's coordinate system [12].

$$\omega_1 = \omega_2 = \omega_3 = \begin{bmatrix} 1 \\ 0 \\ 0 \end{bmatrix}$$

$$q_1 = \begin{bmatrix} 0 \\ 0 \\ 0 \end{bmatrix}; q_2 = \begin{bmatrix} 0 \\ 200 \\ 0 \end{bmatrix}; q_3 = \begin{bmatrix} 0 \\ 400 \\ 0 \end{bmatrix}$$

where the length units are microns

$$g_{st}(\theta) = e^{\hat{\zeta}_1 \theta_1} e^{\hat{\zeta}_2 \theta_2} \dots e^{\hat{\zeta}_n \theta_n} g_{st}(0) \quad (8)$$

$$g_{s1}(0) = \begin{bmatrix} I & \begin{bmatrix} 0 \\ 100 \\ 0 \end{bmatrix} \\ 0 & 1 \end{bmatrix}; g_{s2}(0) = \begin{bmatrix} I & \begin{bmatrix} 0 \\ 300 \\ 0 \end{bmatrix} \\ 0 & 1 \end{bmatrix}; g_{s3}(0) = \begin{bmatrix} I & \begin{bmatrix} 0 \\ 500 \\ 0 \end{bmatrix} \\ 0 & 1 \end{bmatrix} \quad (9)$$

The geometric interpretation of the kinematics is that the current rigid body configuration is equivalent to moving the initial configuration of the rigid body through a screw motion by an amount  $\theta$ . The twist,  $\zeta$ , is an infinitesimal screw motion that is defined in Eq. 10.

$$\hat{\zeta}_i = \begin{bmatrix} \hat{\omega}_i & -\omega_i \times q_i \\ 0 & 0 \end{bmatrix}$$

$$\hat{\omega}_i = \begin{bmatrix} 0 & -\omega_{i,z} & \omega_{i,y} \\ \omega_{i,z} & 0 & -\omega_{i,x} \\ -\omega_{i,y} & \omega_{i,x} & 0 \end{bmatrix} \quad (10)$$

#### Accordion Origami Dynamics

The Newton-Euler equations of motion in body coordinates are given in Eq. 11. The bending stiffness of the bilayer manifests itself in the system of equations as a 3x3 equivalent torsional stiffness matrix,  $K$ . The equivalent moment at the joint due to the drag forces of the moving origami is represented in the 3x3 diagonal matrix  $B$ . The mass, Coriolis, stiffness, and drag matrices are defined below. In the Appendix, the specific terms are described in detail for the accordion model presented above.

$$M(\theta)\ddot{\theta} + C(\theta, \dot{\theta})\dot{\theta} + N(\theta, \dot{\theta}) = \tau \quad (11)$$

$$N(\theta, \dot{\theta}) = K\theta + B\dot{\theta}|\dot{\theta}|$$

$$M(\theta) = \sum_{i=1}^3 J_i^T(\theta) M_i J_i(\theta)$$

$$C_{ij}(\theta, \dot{\theta}) = \sum_{k=1}^n \Gamma_{ijk} \dot{\theta}_k = \frac{1}{2} \sum_{k=1}^n \left( \frac{\partial M_{ij}}{\partial \theta_k} + \frac{\partial M_{ik}}{\partial \theta_j} - \frac{\partial M_{kj}}{\partial \theta_i} \right) \dot{\theta}_k$$

$$K = \begin{bmatrix} k & 0 & 0 \\ 0 & k & 0 \\ 0 & 0 & k \end{bmatrix} \text{ where } k = w \left( \frac{E_1 t_1^3}{3l} + \frac{E_2 t_2^3}{3l} \right)$$

$$B = \begin{bmatrix} b & 0 & 0 \\ 0 & b & 0 \\ 0 & 0 & b \end{bmatrix} \text{ where } b = \frac{1}{16} C_D v_{air} A L^3$$

### Open Loop Control Law

The obvious first step in the control of origami is to simulate the forward dynamics of the structure to an input torque defined by the manufacturing processes. For closed-loop topologies, such as the corner cube, this is a critical step since the hinge design parameters are not immediately evident due to the parallel constraints. The open loop control law for the 3-segment accordion origami is described here with a realistic model of the input forces.

### Step Input

The KOH etch procedure is an event that incrementally releases the stressed bilayer hinge. If the KOH were to etch the silicon immediately, then the turn angle would instantly fold to its final value. This represents a step input, where the open loop control law is given in (12).

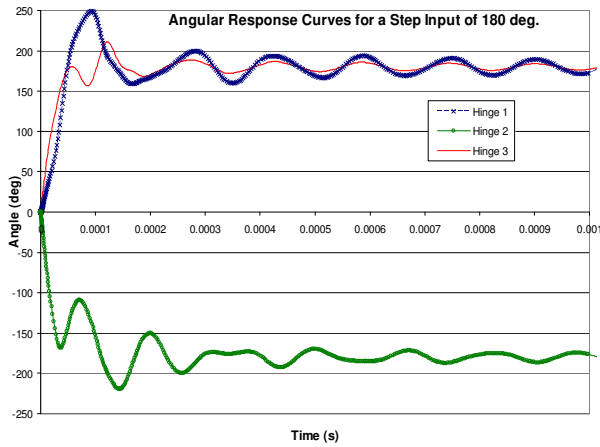


Fig. 7 Step response for accordion model

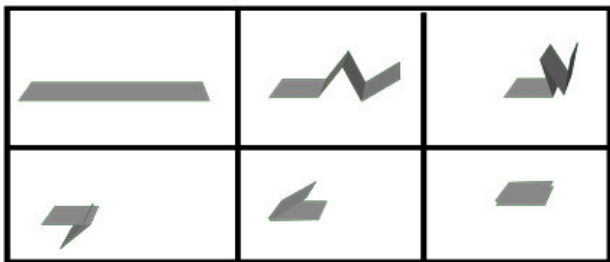


Fig. 8 Trajectory of origami after step input

$$\tau = M(\theta_{des}) \ddot{\theta}_{des} + C(\theta_{des}, \dot{\theta}_{des}) \dot{\theta}_{des} + N(\theta_{des}, \dot{\theta}_{des})$$

$$\theta_{des} = \begin{bmatrix} pi \\ -pi \\ pi \end{bmatrix} \text{ for a step input, which reduces to:}$$

$$\tau = K \theta_{des} \quad (12)$$

The angular response to the step input can be seen in Fig. 7. Note that joint 1 overshoots by about 39%, and the rise times for joints 1-3 are 37 $\mu$ s, 101 $\mu$ s, and 38 $\mu$ s, respectively. This fast response is due to the low mass of the thin films. Figure 8 illustrates screen shots from an animation of the step response of the 3-segment accordion.

The step response represents the system's dynamics when subject to any actuation method governed by Eq. 12. This is not a very realistic model of the experimental behavior, however, since the etch rate is finite.

### Ramp Input

A more accurate input model defines the input joint torques as a function of the etch rate. Since the KOH etch is highly directional along the <1 0 0> crystal plane of Si, the devices can be situated such that the KOH etches along the length of the hinge linearly over time. Figure 9 illustrates the orientation of the device with respect to the etch direction.

Recalling that the turn angle,  $\theta$ , at each joint is related to the length,  $l$ , of the hinge by  $l = \rho \theta$ , it follows that the constant etch rate,  $\beta$ , is equivalent to the time derivative of  $l$ . Therefore, Eq. 13 dictates the open loop control law for a constant etch rate. Not surprisingly, the control law is a ramp input over time period  $T = l / \beta$ , which is approximately 2-3 hours for  $\beta = 1.5 \mu\text{m}/\text{min}$ .

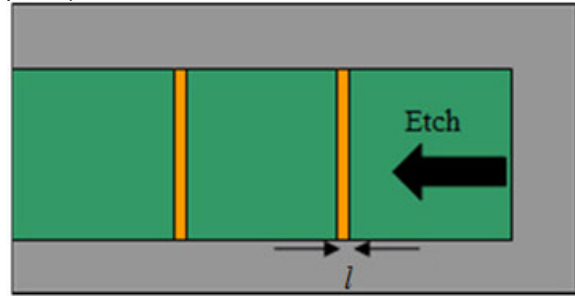


Fig. 9 Schematic of etch process; green: silicon nitride; orange: chromium hinge; gray: silicon

$$\frac{dl}{dt} = \beta = \rho \dot{\theta}_{des}$$

$$\theta_{des} = \int_0^T \frac{\beta}{\rho} dt = \begin{bmatrix} 10\pi T \\ -10\pi T \\ 10\pi T \end{bmatrix} \text{ for a ramp input of } 0.1 \text{ s and } \theta_{final} = \pi$$

$$\tau = M(\theta_{des}) \ddot{\theta}_{des} + C(\theta_{des}, \dot{\theta}_{des}) \dot{\theta}_{des} + N(\theta_{des}, \dot{\theta}_{des}) \quad (13)$$

$$\tau = K \theta_{des} + B \dot{\theta}_{des}^2$$

However, it is not necessary to solve the equations of motion over such a long time period if the response at faster times is still acceptable. The plots in Fig. 10 are the responses of each joint to a ramp input over 0.1 s, which is much faster than the KOH etch. There is minimal overshoot, and the trajectory is very well-behaved, as expected. Longer time periods exhibit improved dynamics, meaning that these simulations are a conservative calculation. Figure 11 displays an animation of the ramp input response.

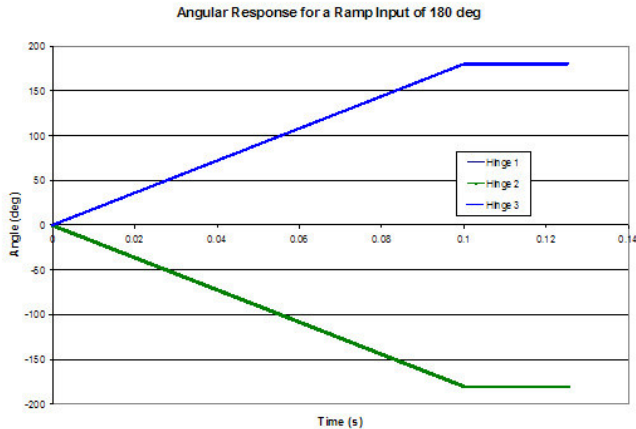


Fig. 10 Ramp response for accordion model

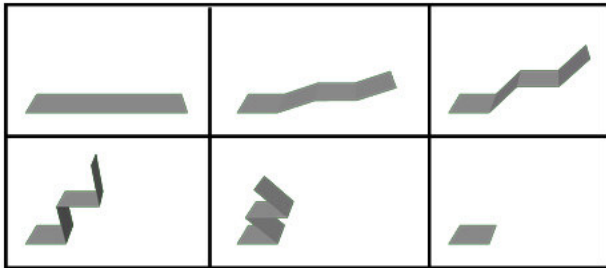


Fig. 11 Trajectory of accordion after ramp input

## CONCLUSIONS

The Nanostructured Origami method is poised to enable new functionality in nanotechnology by patterning membranes in 2D and folding them into 3D. Before complex devices can be fabricated, questions concerning the design and control of origami should be considered. The unfolding of single vertex origami through energy methods introduces a novel way to characterize the geometry of an arbitrary origami. The results in this paper show that it is possible to determine, for at least one class of origami, whether a design is a feasible one from a geometric standpoint. For multiple vertex origami, a similar method could be used to optimize actuation orders such that neighboring segments do not collide or to determine foldability

like in the case of single vertex origami [14]. Understanding the dynamics of the actuation is also important. The results from the accordion model indicate that the stress actuation technique is ideal due to the finite etch rate. By employing methods that are typically used in the robotics community, it is also possible to design an actuation scheme for more complex structures such as the corner cube and other structures with a closed-loop topology.

## REFERENCES

- [1] Qi, M.H. et al. "A three-dimensional optical photonic crystal with designed point defects." *Nature*, 429(6991):538, 2004.
- [2] Jurga, S.M. "3D micro and nanomanufacturing via folding of 2D membranes," M.S. Thesis. In *Dept. of Mechanical Engineering*. Cambridge: Massachusetts Institute of Technology, 2003, pp. 130.
- [3] Demaine, E.D. "Folding and Unfolding." Ph.D. Thesis. In *Dept. of Computer Science*. University of Waterloo, Canada.
- [4] Hastings, J.T., Zhang, F. and Smith, H.I. "Nanometer-level stitching in raster-scanning electron-beam lithography using spatial-phase locking," *Journal of Vacuum Science & Technology B*, vol. 21, pp. 2650-2656, 2003.
- [5] Connelly, R., Demaine, E., and Rote, G. "Straightening polygonal arcs and convexifying polygonal cycles." in *Proceedings of the 41st Annual Symposium on Foundations of Computer Science (FOCS 2000)*, Redondo Beach, California, November 12-14, 2000, pages 432-442.
- [6] Connelly, R., Demaine, E., and Rote, G. "Straightening polygonal arcs and convexifying polygonal cycles." *Discrete and Comp. Geometry*, 30 (2): 205-239, September 2003.
- [7] Streinu, I. "A combinatorial approach to planar non-colliding robot arm motion planning." In *Proc. 41<sup>st</sup> Annual IEEE Sympos. Found. Comput. Sci.* IEEE, November 2000. 443-453.
- [8] Cantarella, J.H., Demaine, E.D., Iben, H.N., and O'Brien, J.F. "An energy-driven approach to linkage unfolding." In *Proceedings of the 20<sup>th</sup> Annual ACM Symposium on Computational Geometry*, Brooklyn, NY, June 2004.
- [9] Streinu, I. and Whiteley, W. "Single-vertex origami and 3-dimensional expansive motions." In *Proc. Japan Conf. Discrete and Comp. Geometry*, Tokai University, Tokyo, Japan, Oct. 8-11, 2004.
- [10] Arora, W., et al. "Nanostructured Origami<sup>TM</sup> 3D Fabrication and Assembly Process Using Strain Actuated Folding." In *The Second International Symposium on Nanomanufacturing*, p. 18, Daejeon, Korea, 2004.
- [11] Arora, W. "Nanostructured Origami<sup>TM</sup>: Folding Thin Films out of the Plane of a Silicon Wafer with Highly Stressed Chromium Hinges." S.M. Thesis. In *Dept. of Electrical*

*Engineering and Computer Science*. Cambridge: Massachusetts Institute of Technology, 2005.

[12] Murray, R.M., Li, Z., and Sastry, S.S., 1994, *A Mathematical Introduction to Robotic Manipulation*. CRC Press: Boca Raton, FL., Ch. 2-5.

[13] In, H.J. et al. "The Nanostructured Origami™ 3D Fabrication and Assembly Process for Nanomanufacturing," IEEE Nanotechnology 2004. Munich, Germany, Aug. 12-14 (paper 8-12).

[14] Esther M. Arkin, Michael A. Bender, Erik D. Demaine, Martin L. Demaine, Joseph S. B. Mitchell, Saurabh Sethia, and Steven S. Skiena, "When Can You Fold a Map?," *Computational Geometry: Theory and Applications*, volume 29, number 1, September 2004, pages 23-46. Special issue of selected papers from the 10th Annual Fall Workshop on Computational Geometry, 2000.

## APPENDIX

The body Jacobian is defined below in terms of instantaneous twists. The adjoint matrix,  $Ad$ , transforms twists in one coordinate frame to twists in another. A full explanation of its usage is given in [12].

$$J_{st}^b(\theta) = [\zeta_1^* \dots \zeta_{n-1}^* \zeta_n^*]$$

$$\zeta_i^* = Ad_{\left( e^{\hat{\zeta}_i \theta_i} \dots e^{\hat{\zeta}_n \theta_n} \right)}^{-1} \zeta_i$$

For the accordion model, the body Jacobians of each link with respect to the inertial frame are:

$$J_1^b(\theta) = [\zeta_1^* \ 0 \ 0] = \begin{bmatrix} 0 & 0 & 0 \\ 0 & 0 & 0 \\ 100 & 0 & 0 \\ 1 & 0 & 0 \\ 0 & 0 & 0 \\ 0 & 0 & 0 \end{bmatrix}$$

$$J_2^b(\theta) = [\zeta_1^* \ \zeta_2^* \ 0] = \begin{bmatrix} 0 & 0 & 0 \\ 200s_2 & 0 & 0 \\ 200c_2 + 100 & 100 & 0 \\ 1 & 1 & 0 \\ 0 & 0 & 0 \\ 0 & 0 & 0 \end{bmatrix}$$

$$J_3^b(\theta) = [\zeta_1^* \ \zeta_2^* \ \zeta_3^*] = \begin{bmatrix} 0 & 0 & 0 \\ 200s_3 + 200c_3s_2 + 200s_3c_2 & 0 & 0 \\ 200c_3 + 200c_3c_2 - 200s_3s_2 + 100 & 200s_3 & 100 \\ 1 & 200c_3 + 100 & 1 \\ 0 & 0 & 0 \\ 0 & 0 & 0 \end{bmatrix}$$

The mass matrix,  $M$ , is given by:

$$M_i = \begin{bmatrix} mI & 0 \\ 0 & I \end{bmatrix}$$

where  $I$  is the 3x3 identity matrix, and  $I$  is the 3x3 inertia matrix.